Fluorescent Biological Probes

DOI: 10.1002/anie.201408476

Specific Light-Up Bioprobe with Aggregation-Induced Emission and Activatable Photoactivity for the Targeted and Image-Guided Photodynamic Ablation of Cancer Cells**

*Youyong Yuan, Chong-Jing Zhang, Meng Gao, Ruoyu Zhang, Ben Zhong Tang, and Bin Liu**

Abstract: *Activatable photosensitizers (PSs) have been widely used for the simultaneous fluorescence imaging and photodynamic ablation of cancer cells. However, the ready aggregation of traditional PSs in aqueous media can lead to fluorescence quenching as well as reduced phototoxicity even in the activated form. We have developed a series of PSs that show aggregation-enhanced emission and phototoxicity and thus the exact opposite behavior to that of previously reported PSs. We further developed a dual-targeted enzyme-activatable bioprobe based on the optimized photosensitizer and describe simultaneous light-up fluorescence imaging and activated photodynamic therapy for specific cancer cells. The design of smart probes should thus open new opportunities for targeted and image-guided photodynamic therapy.*

The combination of diagnostic and therapeutic capabilities within a single formulation is highly desirable for personalized medicine in the treatment of cancer.[1] Image-guided therapies have the ability to provide early personalized diagnosis and subsequent specific therapy to maximize therapeutic efficiency with reduced side effects. As most chemotherapeutic drugs are non-emissive, they often need to be conjugated with fluorescent tags to enable them to be traced, which may affect the pathway and distribution of the original drugs. Furthermore, cell resistance toward conventional chemotherapeutic drugs and the side effects of these drugs on healthy tissues has stimulated the further development of new therapeutic modalities. In this regard, photodynamic therapy (PDT) has emerged as a noninvasive and reliable cancer-therapy modality with high spatiotemporal precision.[2] For PDT, photosensitizers (PSs) that are able to generate toxic reactive oxygen species (ROS) to induce cell death upon irradiation with light play a key role. More importantly, the inherent fluorescence of PSs offers an opportunity for image-guided therapy. Recently, activatable PSs have been developed to further minimize the side effects of PDT and to increase the signal-to-background ratio for bioimaging.[3] The design is generally based on the concept that the prequenched fluorescence and inhibited phototoxicity of the PS could be restored once a specific trigger is able to separate the quencher or energy acceptor from the vicinity of the PS.[3] However, as most PSs are hydrophobic, they would naturally aggregate in aqueous media through π–π stacking owing to their rigid planar structures. The aggregation of activated PSs can lead to fluorescence quenching and reduced phototoxicity and thus affects the quality of imaging and the effect of PDT.[4] As aggregation is an intrinsic process for hydrophobic PSs in aqueous media, it is highly desirable to develop novel PSs that show enhanced fluorescence and phototoxicity in the aggregate state.

Propeller-shaped fluorogens that show aggregation-induced emission (AIE), such as tetraphenylethene (TPE) and silole derivatives, have recently attracted great research interest in the areas of biosensing, imaging, and therapy.[5] These fluorogens are non-emissive in the molecularly dissolved state but induced to emit strong fluorescence in the aggregation state owing to the restriction of intramolecular rotation (RIR) and prohibition of energy dissipation through nonradiative channels.[6] As compared to traditional fluorogens, including PSs, which show a notorious phenomenon known as aggregation-caused quenching (ACQ) at high concentrations,[7] fluorogens with AIE characteristics can serve as a distinct alternative tool for the design of light-up probes.[5e–g,8] These unique properties inspired us to develop novel and activatable photosensitizer probes based on an AIE fluorogens for image-guided photodynamic therapy.

Cathepsin B is a lysosomal protease overexpressed in many types of tumors.[9] It can specifically cleave substrates with a -Gly-Phe-Leu-Gly- (GFLG) peptide sequence and has been used for enzyme-responsive drug delivery.[10] On the other hand, cyclic arginine–glycine–aspartic acid (cRGD), which can selectively interact with $\alpha_v\beta_3$ integrin overex-

[*] Dr. Y. Yuan,[+] Dr. C. Zhang,[+] R. Zhang, Prof. Dr. B. Liu
Department of Chemical and Biomolecular Engineering
National University of Singapore
4 Engineering Drive 4, Singapore, 117585 (Singapore)
E-mail: cheliub@nus.edu.sg
Dr. M. Gao, Prof. Dr. B. Liu
Institute of Materials Research and Engineering
3 Research Link, Singapore, 117602 (Singapore)
Prof. Dr. B. Z. Tang
Department of Chemistry, Division of Biomedical Engineering
The Hong Kong University of Science and Technology
Clear Water Bay, Kowloon, Hong Kong (China)
and
SCUT-HKUST Joint Research Laboratory, Guangdong Innovative Research Team, State Key Laboratory of Luminescent Materials and Devices, South China University of Technology
Guangzhou, 510640 (China)
[+] These authors contributed equally.

[**] We thank the Ministry of Defense (R279-000-340-232), SMART (R279-000-378-592), the Ministry of Education (R279-000-391-112) and the Institute of Materials Research and Engineering of Singapore (IMRE/12-8P1103), the Research Grants Council of Hong Kong (HKUST2/CRF/10 and N HKUST620/11), and the Guangdong Innovative Research Team Program (201101C0105067115) for financial support.
Supporting information for this article is available on the WWW under http://dx.doi.org/10.1002/anie.201408476.

pressed in cancer cells, has been used for targeted drug delivery.[11] By incorporating a target ligand and a substrate that can be cleaved by cathepsin B to give an activatable probe, it should be possible to achieve highly specific cancer-cell killing as a result of the dual selection processes.

In this study, we developed a simple but unique bioprobe based on a newly developed AIE fluorogen that can be utilized for the target-specific light-up imaging and activatable photodynamic ablation of cancer cells (Scheme 1). The probe is composed of four parts: 1) an orange fluorescent AIE fluorogen as an imaging reagent and photosensitizer, 2) a GFLG peptide substrate that is responsive to cathepsin B, 3) a hydrophilic linker with three Asp (D) units to increase the hydrophilicity of the probe, and 4) a cRGD-targeting moiety. The probe is almost nonfluorescent with a very low ROS-generation ability in aqueous media owing to the consumption of excitonic energy by free intramolecular motions. After cancer-cellular uptake, cleavage of the GFLG substrate by cathepsin B will lead to enhanced fluorescence signal output concomitant with activated photoactivity for image-guided PDT. Therefore, the probe design offers a good opportunity to develop activatable PSs without incorporating any quencher or energy acceptor. Enhanced fluorescence and phototoxicity is then observed in the aggregate state upon activation by tumor-related stimuli.

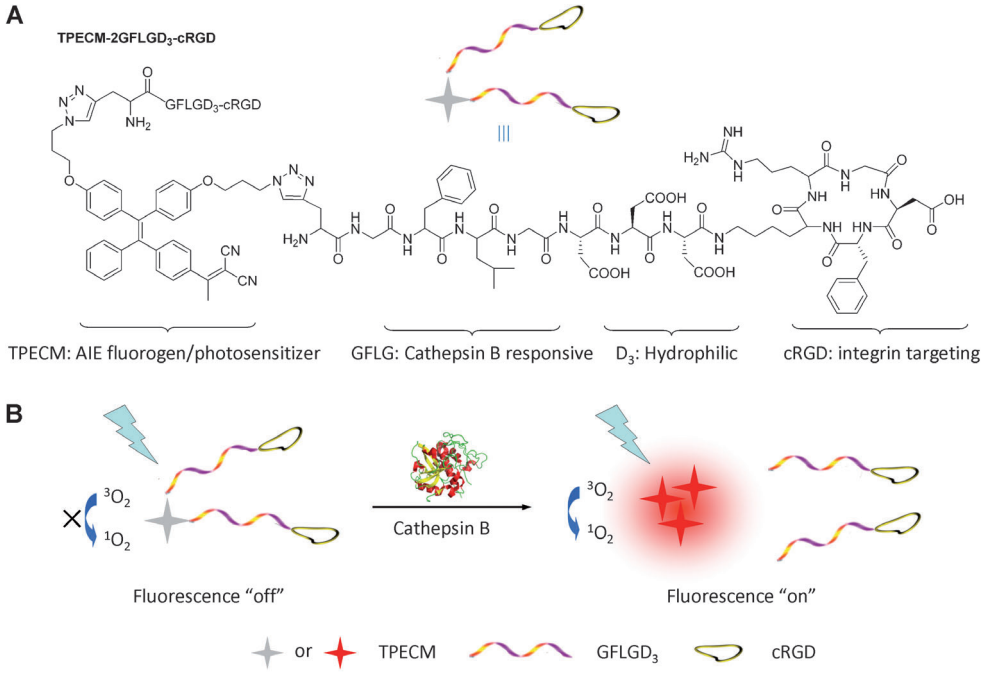

Scheme 1. A) Synthetic route to the functionalizable TPE derivative TPECM-2N_3 and the bioprobe TPECM-2GFLGD_3-cRGD. B) Schematic illustration of probe activation by cathepsin B with fluorescence "turn-on" and activated photoactivity to generate reactive oxygen species (ROS) upon irradiation with light.

TPE, with an absorption maximum at 310 nm, is the most commonly used blue-emissive AIE fluorogen. The incorporation of dicyanovinyl groups into TPE recently yielded molecules that were reported to show visible absorption with orange to red emission.[12] We first synthesized several dicyanovinyl-containing AIE fluorogens (see Scheme S1 and Figures S1–S10 in the Supporting Information). We found that a compound with a simple dicyanovinyl group reacted with biological thiol molecules (see Figure S11) and could efficiently generate ROS upon irradiation with light (see Figure S12). The reactivity with biothiols could change the optical properties of these fluorogens. To reduce the reactivity of the dicyanovinyl group towards biothiols, we synthesized three new AIE fluorogens with different substituents attached to the dicyanovinyl group. We speculated that the larger size of the substituent would increase steric effects to reduce its reactivity with biothiols. None of the three compounds showed detectable reactivity toward common biothiols at room temperature (see Figures S13 and S14). An increase in the size of the substituent was found to lead to a blue shift in both the absorption and emission spectra (see Figure S15). Fluorogen **1** was selected for the subsequent study because it shows orange–red emission in aggregates and can be excited by both 405 and 457 nm lasers.

The synthetic route to TPECM-2GFLGD_3-cRGD is shown in Scheme 1. The azide-functionalized TPE derivative (TPECM-2N_3) was synthesized from AIE fluorogen **2**. Compound **2** was treated first with tribromoborane and then with an azide-containing linker to give **3**. A reaction between **3** and malononitrile on a SiO_2 support yielded TPECM-2N_3. Subsequent coupling between TPECM-2N_3 and alkyne-functionalized GFLGD_3-cRGD through a "click" reaction afforded the probe TPECM-2GFLGD_3-cRGD after HPLC purification. The probe was characterized thoroughly to confirm its structure and high purity (see Figures S16 and S17).

It is known that TPE shows typical characteristics of AIE fluorogens;[6] that is, it is non-emissive in the molecularly dissolved state, but emits strongly in the solid state or as an aggregate in a poor solvent. To test whether the dicyanovinyl-modified TPE derivative retained the AIE properties, we studied the fluorescence intensity of TPECM-2N_3 in dimethyl sulfoxide (DMSO)/water mixtures with different water fractions (f_w). TPECM-2N_3 was found to be almost nonfluorescent as a solution in DMSO ($f_w = 0$; Figure S18). However, as the f_w value increased, the fluorescence intensity increased steadily. At $f_w = 99\,\%$, the fluorescence intensity reached a maximum and was 105 times higher than that in DMSO. The increase in fluorescence intensity indicated that TPECM-2N_3

tended to aggregate when the f_w value increased, thus resulting in restriction of the intramolecular motion. The aggregate formation of TPECM-$2N_3$ was also confirmed by laser-light scattering (LLS; ee Figure S19 A). These results indicate that dicyanovinyl-modified TPE retains its AIE properties. The UV/Vis absorption spectra of TPECM-$2N_3$ and the probe in DMSO/buffer (1:199, v/v) are shown in Figure S19 B of the Supporting Information. The probe shows a similar absorption profile in the 350–520 nm range to that of TPECM-$2N_3$. However, their emission spectra are very different: TPECM-$2N_3$ shows intense orange fluorescence, whereas the probe is almost nonfluorescent in the same medium owing to its good water solubility (Figure 1 A). The probe is also stable and remains nearly nonfluorescent in DMEM medium or in PBS buffer with a high ionic strength (0–960 mM) and at pH 7.4 to 5.0 (see Figure S20). The probe maintains an "off" state in complex media, which indicates its great potential to serve as a specific light-up probe with minimal background interference.

The response of the probe to cathepsin B was monitored by reverse-phase HPLC. After activation, the AIE residue had a longer retention time (see Figure S21), thus indicating that it was more hydrophobic than the probe itself. The increased hydrophobicity could lead to an increase in fluorescence intensity owing to aggregation of the cleaved residues in aqueous media. The fluorescence change of the probe incubated with cathepsin B was monitored over time in DMSO/buffer (1:199, v/v). A quick and steady fluorescence increase of the probe solution was observed upon the addition of cathepsin B, and a plateau corresponding 35-fold higher fluorescence than the intrinsic emission of the probe was reached after incubation for 60 min (Figure 1 B). Subsequently, we also incubated the probe at different concentrations with cathepsin B for 60 min and studied the corresponding fluorescence intensity. A plot of the PL intensity at 615 nm against the probe concentration gave a linear line ($R^2 = 0.99$; see Figure S22), thus suggesting the possibility of quantifying cathepsin B by monitoring the change in PL intensity. The enzymatic efficiency (k_{cat}/K_M) was calculated to be approximately 142 $M^{-1}s^{-1}$ (see Figure S23), which shows a reasonable degradation efficiency of the -GFLG- linker by cathepsin B.[10b] The molecular dissolution of the probe and the aggregate formation of the cleaved residues were confirmed by LLS measurements and atomic force microscopy (AFM). In the aqueous mixture, no LLS signals could be detected from the solution of the probe. However, after treatment with cathepsin B, the hydrophobic AIE residue tended to cluster into aggregates (see Figure S24), as also confirmed by AFM. Aggregate formation clearly explains the probe fluorescence turn-on in the presence of cathepsin B.

Probe-selectivity studies showed that only cathepsin B could activate the probe, whereas GSH, cysteine, and several other biomolecules (e.g. 10 mg mL^{-1} BSA) did not cause any evident fluorescence change (see Figure S25). These results demonstrate that the probe has the potential to be activated in cancer cells in the presence of overexpressed cathepsin B. To test this hypothesis, we obtained the cell lysate of cells with and without pretreatment with CA-074-Me, a cell-permeable inhibitor that can suppress the biological activity of cath-

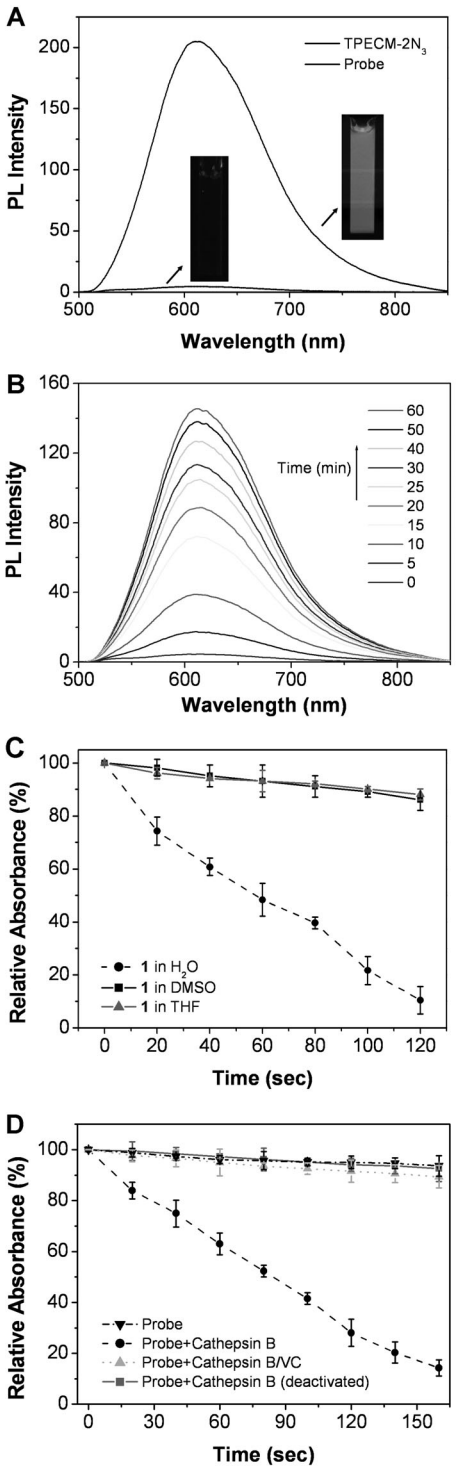

Figure 1. A) Photoluminescence (PL) spectra of TPECM-$2N_3$ and the probe in DMSO/buffer (1:199, v/v; pH 5.0). Inset: Corresponding photographs taken under illumination by a UV lamp at 365 nm. B) Time-dependent fluorescence spectra of the probe (5 μM) in the presence of cathepsin B (1 μg mL^{-1}) in DMSO/buffer (1:199, v/v). C) Plots of the relative absorbance change of DPBF at 418 nm versus irradiation time in the presence of compound **1** in water, THF, or DMSO. D) Plots of the relative absorbance change versus irradiation time of the probe (5 μM) alone, with cathepsin B (1 μg mL^{-1}, 60 min) in the absence and presence of vitamin C (VC), and with the same amount of deactivated cathepsin B. The data shown are mean values ± standard deviation, $n = 3$.

epsin B. The cell lysates of cancer cells MDA-MB-231 and MCF-7 as well as normal 293T cells with low expression of cathepsin B[13] were obtained and directly incubated with the probe. Only cancer cells showed a significant fluorescence increase; normal cells and cancer cells pretreated with CA-074-Me showed only a limited increase in fluorescence (see Figure S26).

The generation of ROS upon the irradiation of a photosensitizer with light is the key step for photodynamic therapy. We first studied the ROS generation of the AIE fluorogen **1** upon irradiation with light by using 1,3-diphenylisobenzofuran (DPBF) and 2′,7′-dichlorodihydrofluorescein diacetate (DCFDA) as the ROS indicators. DPBF can readily undergo 1,4-cycloaddition reactions with ROS, which results in decreased absorbance at 418 nm, whereas DCFDA is non-fluorescent but can be rapidly oxidized by ROS to the fluorescent molecule dichlorofluorescein (DCF). Compound **1** can generate ROS efficiently in water upon irradiation with light (Figure 1 C). However, its ROS-generation capability is much weaker in DMSO or THF under the same conditions, in accordance with its fluorescence properties. The ROS-generation ability of the probe with or without cathepsin B pretreatment was also studied. In the presence of the probe alone, the absorbance of DPBF at 418 nm decreased slightly by less than 10 % during irradiation with light for 160 s (Figure 1 D). However, when the probe was pretreated with cathepsin B, the DPBF absorbance decreased by more than 85 % under identical conditions. Furthermore, the absorbance of DPBF showed only a minimal decrease when the ROS scavenger vitamin C was added or when deactivated cathepsin B was used. The absorbance of the probe at 418 nm does not contribute to the measured absorbance change owing to its very low concentration (see Figure S27). These ROS-generation differences were also confirmed by using DCFDA as the indicator. It was found that ROS generation was not susceptible to subtle alterations in the pH value (see Figure S28 A,B). However, the generation of ROS was dependent on the power of the laser, which offers the potential to control therapy by irradiation with an external light (see Figure S28 C). These results confirm that the probe itself shows low ROS generation, but that the phototoxicity can be significantly enhanced by cleavage of the probe by cathepsin B.

To demonstrate cell-specific light-up imaging, we incubated the probe with MDA-MB-231 cells overexpressing $\alpha_v\beta_3$ integrin and used MCF-7 and 293T cells as negative controls.[11] Upon incubation with the probe, the red fluorescence in MDA-MB-231 cells intensified gradually as the incubation time increased, and reached a maximum after incubation for 4 h (see Figure S29). The signal in MDA-MB-231 cells was much stronger than those in MCF-7 and 293T cells after the same period of time (Figure 2). However, when MDA-MB-231 cells were pretreated with free cRGD and/or CA-074-Me prior to probe incubation, the fluorescence intensity decreased dramatically, probably as a result of inefficient cellular uptake and/or poor probe activation. The specific fluorescence light-up of the probe in cells was also confirmed by flow cytometry analysis (see Figure S30), which revealed receptor-mediated probe uptake by MDA-MB-231 cells. Furthermore, the fluorescence intensity in the cells intensified when the probe was incubated at a higher concentration, thus indicating the potential for semiquantification of the activated AIE probe inside cells (see Figure S31).

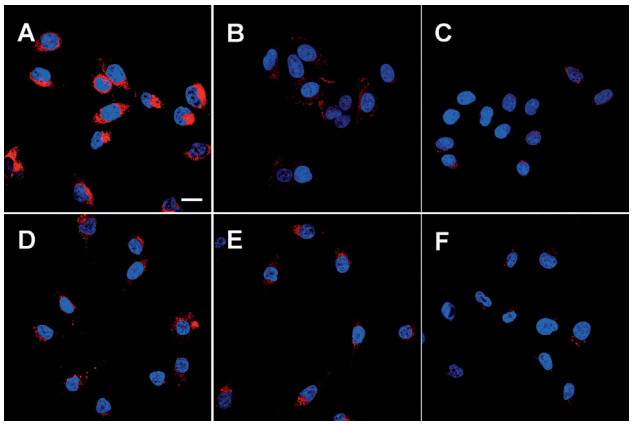

Figure 2. Confocal images of A) MDA-MB-231 cells, B) MCF-7 cells, C) 293T cells, D) MDA-MB-231 cells pretreated with free cRGD, E) MDA-MB-231 cells pretreated with CA-074-Me, and F) MDA-MB-231 cells pretreated with both cRGD and CA-074-Me after incubation with the probe (5 μM) for 4 h. The blue fluorescence is from the cell nuclei dyed with 4′,6-diamidino-2-phenylindole (DAPI; $E_x = 405$ nm; $E_m = 430$–470 nm), the red fluorescence is from the probe ($E_x = 405$ nm; $E_m > 560$ nm). All images share the same scale bar (20 μm).

It has been reported that cathepsin B is a lysosomal protease.[14] To identify the activation location of the probe after cellular uptake, colocalization experiments were performed with the commercially available fluorescent lysosome-selective marker Lysotracker Green DND-26. The red fluorescence colocalized well with the green fluorescence from Lysotracker Green in MDA-MB-231 cells (Figure 3 A–D). Therefore, we can conclude that the probe activation largely occurs in the lysosome to yield the fluorescence "turn-on". It has been reported that PSs localized in the lysosome could damage the lysosome and induce cell apoptosis upon irradiation with light.[15] To verify the damage by ROS upon irradiation with light, we used acridine orange as the cell-permeable indicator to study the integrity of the acidic organelles. Acridine orange emits red fluorescence in acidic organelles, such as lysosomes, and displays green fluorescence in the cytoplasm and nucleus. When there was no evident ROS generation, the MDA-MB-231 cells displayed both red and green fluorescence (Figure 3 E,F), thus indicating that the lysosomes were not damaged. However, when the cells were incubated with the probe and irradiated with white light for 1 min ($0.25\ W\,cm^{-2}$), the red fluorescence from acridine orange was remarkably reduced (Figure 3 G), thus indicating that the lysosomes were destroyed. Accordingly, a longer irradiation time led to a clearer decrease in red fluorescence (Figure 3 H). These results demonstrate that the probe could be activated in the lysosome and damage the lysosome membranes upon irradiation with light.

Annexin V tagged with fluorescein isothiocyanate (FITC) is one of the most commonly used fluorescent probes to distinguish viable cells from apoptotic cells because Annex-

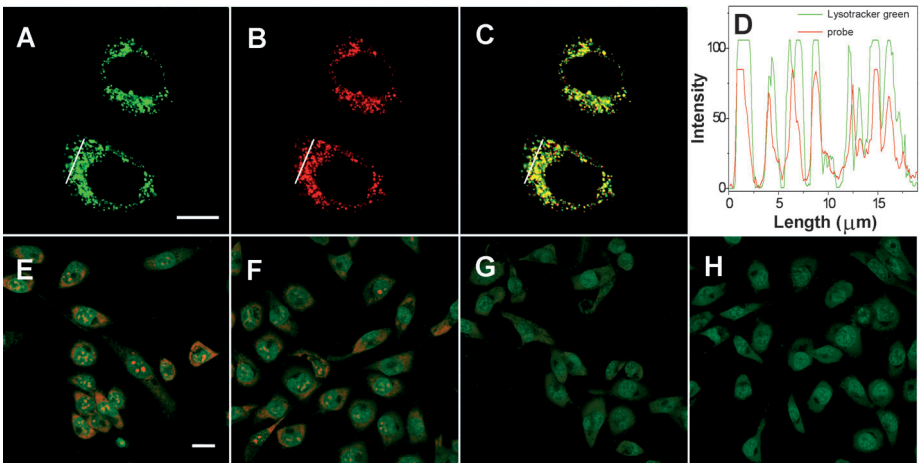

Figure 3. A–D) Subcellular localization of the probe in MDA-MB-231 cells. A) Fluorescence image of cells treated with Lysotracker Green DND-26 (E_x: 488 nm; E_m: 505–525 nm). B) Fluorescence image of cells treated with the probe (E_x = 405 nm; E_m > 560 nm). C) Overlay of images (A) and (B). D) Correlation of the probe and DND-26 intensities (green: Lysotracker Green, red: probe). E–H) Observation of lysosomal disruption of MDA-MB-231 cells as induced by the probe upon irradiation with light in the presence of acridine orange (5 μM) as the indicator. The cells were treated with E) light only, F) the probe without irradiation, G) the probe with light irradiation for 1 min, H) the probe with light irradiation for 2 min. E_x = 488 nm; E_m = 505–525 (green) or 610–640 nm (red). Images (A–C) and (E–H) all share the same scale bar (20 μm).

in V can selectively bind to the membrane of apoptotic cells, which express phosphatidylserine. After the incubation of MDA-MB-231 cells with the probe for 4 h, followed by irradiation with light, green fluorescence was clearly observed from the cell membrane (Figure 4), thus indicating that the cells underwent apoptosis. No significant FITC signal was detectable in MCF-7 cells, 293T cells, or MDA-MB-231 cells pretreated with cRGD or CA-074-Me or vitamin C, thus revealing little or no apoptosis. These results agree well with the ROS-generation studies with DCFDA as the indicator (see Figure S32).

A practical system for phototherapy should exhibit low cytotoxicity before light irradiation and is able to induce a high percentage of cell death upon exposure to light. We first evaluated the cytotoxicity of the probe to MDA-MB-231, MCF-7, and 293T cells upon incubation in the dark by a standard MTT assay. After incubation for 24 h, no significant cytotoxicity was observed for any of the tested cells, even when the probe concentration reached 50 μM (Figure 5A). However, upon irradiation with light, a dose-dependent cytotoxicity was observed in MDA-MB-231 cells (Figure 5B). In parallel experiments with MCF-7 and 293T cells under identical conditions, only minimal toxicity was observed. The half-maximal inhibitory concentration (IC_{50}) of the probe for MDA-MB-231 cells was 3.05 μM under the experimental conditions. However, when MDA-MB-231 cells were pretreated with cRGD, CA-074-Me, or vitamin C, decreased cell death was observed (Figure 5C), in agreement with the apoptosis studies. Furthermore, to validate the proposed time-controlled PDT, the probe-stained MDA-MB-231 cells were exposed to irradiation with light for different durations. With a longer laser irradiation time, stronger inhibition of cell viability was observed (Figure 5D). These results indicate that the phototherapy can also be regulated by the probe concentration as well as the laser irradiation time.

In summary, we have reported the synthesis and biological evaluation of a bioprobe based on a new AIE fluorogen for the targeted light-up imaging and photodynamic ablation of cancer cells. The specific probe activation enables real-time and light-up cancer-cell imaging with a high signal-to-noise ratio. The dual-targeted design strategy also led to the highly selective ablation of cancer cells. As compared to existing activatable PSs, our probe design is simple but effective. It does not involve any quencher or energy acceptor, yet it shows a high signal-to-noise ratio. Furthermore, in contrast to traditional PSs, which show aggregation-caused quenching, our probe shows unique aggregation-induced emission and ROS generation upon enzyme activation. However, although the developed bioprobe functioned well in in vitro studies, it has the limitation of short-wavelength excitation, which precludes practical applications at the moment. On the basis of the proof-of-concept bioprobe design, further molecular development to endow the AIE fluorogens with long absorption wavelengths or large two-photon-absorption cross-sections is likely to yield a new generation of probes with activatable

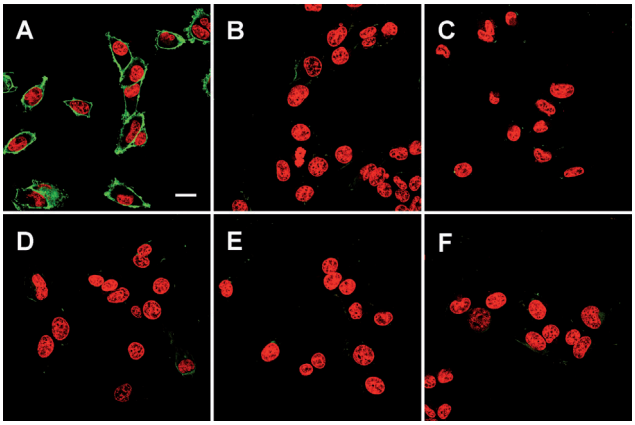

Figure 4. Imaging of cell apoptosis with FITC-tagged Annexin V in A, D, E, F) MDA-MB-231 cells, B) MCF-7 cells, and C) 293T cells after incubation of the cells with the probe (5 μM) for 4 h, followed by irradiation with white light (0.25 $W cm^{-2}$). For (D), (E), and (F), the MDA-MB-231 cells were pretreated with cRGD (D), CA-074-Me (E), or vitamin C (F). The nuclei of the living cells were stained with DRAQ5 (E_x = 633 nm; E_m > 650 nm), the green fluorescence is from FITC (E_x = 488 nm; E_m = 505–525 nm). All images share the same scale bar (20 μm).

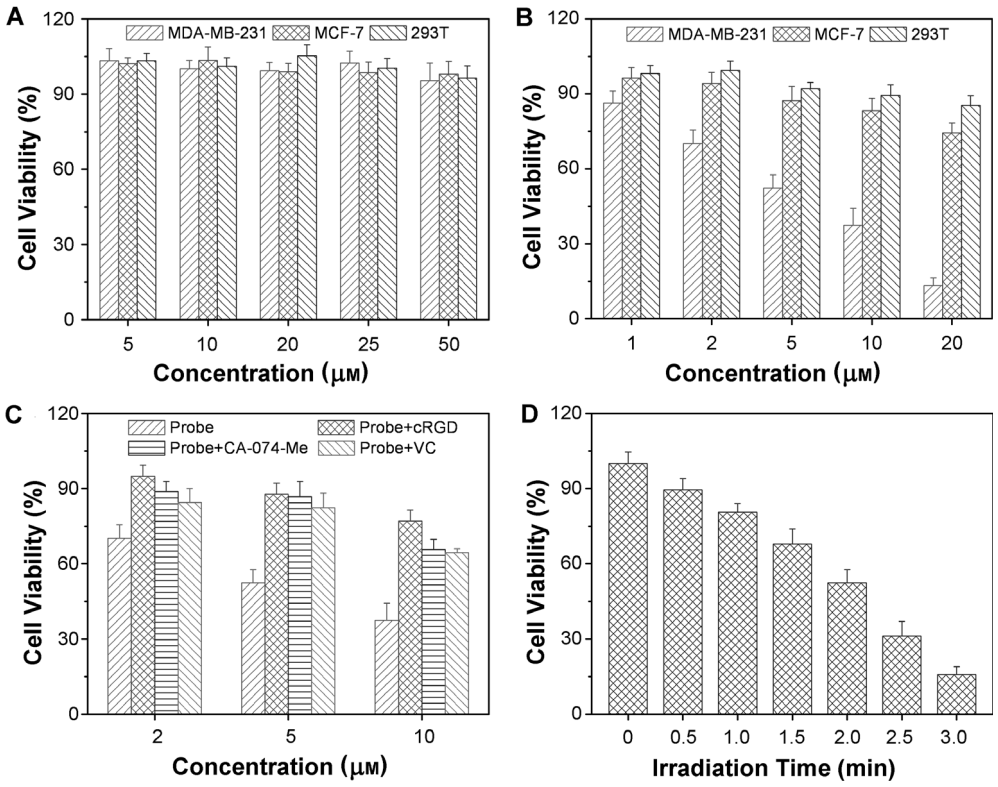

Figure 5. A) Cell viability of MDA-MB-231, MCF-7, and 293T cells upon treatment with the probe at different concentrations in the dark for 24 h. B) Inhibition of the growth of MDA-MB-231, MCF-7, and 293T cells in the presence of the probe at different concentrations upon light irradiation (0.25 Wcm^{-2}, 2 min) followed by further incubation of the cells for 24 h. C) Viability of MDA-MB-231 cells incubated with the probe after pretreatment with free cRGD, CA-074-Me, or VC, followed by irradiation with light (0.25 Wcm^{-2}, 2 min) and further incubation for 24 h. Cells incubated with the probe were used as a control. D) Inhibition of MDA-MB-231 cell growth upon incubation of the cells with the probe (5 μM) and irradiation with light (0.25 Wcm^{-2}) for different periods of time, followed by further incubation for 24 h. The data shown are mean values ± standard deviation, $n = 3$.

fluorescence and photoactivity for image-guided PDT in vivo; such studies are being actively pursued in our laboratory.

Received: August 23, 2014
Revised: November 19, 2014
Published online: December 11, 2014

Keywords: aggregation-induced emission (AIE) · cancer · fluorescence imaging · image-guided therapy · photodynamic therapy

[1] J. V. Jokerst, S. S. Gambhir, *Acc. Chem. Res.* **2011**, *44*, 1050–1060.

[2] D. E. Dolmans, D. Fukumura, R. K. Jain, *Nat. Rev. Cancer* **2003**, *3*, 380–387.

[3] a) J. F. Lovell, T. W. Liu, J. Chen, G. Zheng, *Chem. Rev.* **2010**, *110*, 2839–2857; b) J. F. Lovell, M. W. Chan, Q. Qi, J. Chen, G. Zheng, *J. Am. Chem. Soc.* **2011**, *133*, 18580–18582; c) J. Tian, L. Ding, H. J. Xu, Z. Shen, H. Ju, L. Jia, L. Bao, J. S. Yu, *J. Am. Chem. Soc.* **2013**, *135*, 18850–18858; d) E. Cló, J. W. Snyder, N. V. Voigt, P. R. Ogilby, K. V. Gothelf, *J. Am. Chem. Soc.* **2006**, *128*, 4200–4201; e) Y. Ichikawa, M. Kamiya, F. Obata, M. Miura, T. Terai, T. Komatsu, T. Ueno, K. Hanaoka, T. Nagano, Y. Urano, *Angew. Chem. Int. Ed.* **2014**, *53*, 6772–6775; *Angew. Chem.* **2014**, *126*, 6890–6893; f) Y. Zhang, J. Qian, D. Wang, Y. L. Wang, S. L. He, *Angew. Chem. Int. Ed.* **2013**, *52*, 1148–1151; *Angew. Chem.* **2013**, *125*, 1186–1189; g) Q. Yuan, Y. Wu, J. Wang, D. Lu, Z. Zhao, T. Liu, X. Zhang, W. Tan, *Angew. Chem. Int. Ed.* **2013**, *52*, 13965–13969; *Angew. Chem.* **2013**, *125*, 14215–14219.

[4] a) L. E. Bennett, K. P. Ghiggino, R. W. Henderson, *J. Photochem. Photobiol. B* **1989**, *3*, 81–89; b) S. Y. Park, H. J. Baik, Y. T. Oh, K. T. Oh, Y. S. Youn, E. S. Lee, *Angew. Chem. Int. Ed.* **2011**, *50*, 1644–1647; *Angew. Chem.* **2011**, *123*, 1682–1685.

[5] a) C. Li, T. Wu, C. Hong, G. Zhang, S. Liu, *Angew. Chem. Int. Ed.* **2012**, *51*, 455–459; *Angew. Chem.* **2012**, *124*, 470–474; b) X. Wang, J. Hu, G. Zhang, S. Liu, *J. Am. Chem. Soc.* **2014**, *136*, 9890–9893; c) D. Ding, K. Li, B. Liu, B. Z. Tang, *Acc. Chem. Res.* **2013**, *46*, 2441–2453; d) K. Li, B. Liu, *Chem. Soc. Rev.* **2014**, *43*, 6570–6597; e) H. Shi, J. Liu, J. Geng, B. Z. Tang, B. Liu, *J. Am. Chem. Soc.* **2012**, *134*, 9569–9572; f) Y. Yuan, R. T. Kwok, B. Z. Tang, B. Liu, *J. Am. Chem. Soc.* **2014**, *136*, 2546–2554; g) X. Xue, Y. Zhao, L. Dai, X. Zhang, X. Hao, C. Zhang, S. Huo, J. Liu, C. Liu, A. Kumar, W.-Q. Chen, G. Zou, X.-J. Liang, *Adv. Mater.* **2014**, *26*, 712–717; h) F. Hu, Y. Huang, G. Zhang, R. Zhao, H. Yang, D. Zhang, *Anal. Chem.* **2014**, *86*, 7987–7995; i) X. Zhang, X. Zhang, L. Tao, Z. Chi, J. Xu, Y. Wei, *J. Mater. Chem. B* **2014**, *2*, 4398–4414; j) C. W. Leung, Y. Hong, S. Chen, E. Zhao, J. W. Lam, B. Z. Tang, *J. Am. Chem. Soc.* **2013**, *135*, 62–65; k) J. Zhang, J. Chen, B. Xu, L. Wang, S. Ma, Y. Dong, B. Li, L. Ye, W. Tian, *Chem. Commun.* **2013**, *49*, 3878–3880; l) S. Kim, T. Ohulchanskyy, H. Pudavar, R. Pandey, P. Prasad, *J. Am. Chem. Soc.* **2007**, *129*, 2669–2675; m) Y. Yuan, G. Feng, W. Qin, B. Z. Tang, B. Liu, *Chem. Commun.* **2014**, *50*, 8757–8760; n) X. Zhang, X. Zhang, S. Wang, M. Liu, Y. Zhang, L. Tao, Y. Wei, *ACS Appl. Mater. Interfaces* **2013**, *5*, 1943–1947.

[6] Y. Hong, J. W. Lam, B. Z. Tang, *Chem. Soc. Rev.* **2011**, *40*, 5361–5388.

[7] J. B. Birks, *Photophysics of Aromatic Molecules*, Wiley, London, **1970**.

[8] a) M. Wang, X. Gu, G. Zhang, D. Zhang, D. Zhu, *Anal. Chem.* **2009**, *81*, 4444–4449; b) A. Shao, Z. Guo, S. Zhu, S. Zhu, P. Shi, H. Tian, W. Zhu, *Chem. Sci.* **2014**, *5*, 1383–1389.

[9] J. Decock, N. Obermajer, S. Vozelj, W. Hendrickx, R. Paridaens, J. Kos, *Int. J. Biol. Markers* **2008**, *23*, 161–1688.

[10] a) R. Duncan, H. Cable, J. Lloyd, P. Rejmanová, J. Kopeček, *Makromol. Chem.* **1983**, *184*, 1997 – 2008; b) P. Rejmanová, J. Kopeček, *Makromol. Chem.* **1983**, *184*, 2009 – 2020.
[11] E. Ruoslahti, *Annu. Rev. Cell Dev. Biol.* **1996**, *12*, 697 – 715.
[12] X. Gu, J. Yao, G. Zhang, C. Zhang, Y. Yan, Y. Zhao, D. Zhang, *Chem. Asian J.* **2013**, *8*, 2362 – 2369.
[13] H. Yoshii, H. Kamiyama, K. Goto, K. Oishi, N. Katunuma, Y. Tanaka, H. Hayashi, T. Matsuyama, H. Sato, N. Yamamoto, Y. Kubo, *PLoS One* **2011**, *6*, e19352.
[14] T. Reinheckel, J. Deussing, W. Roth, C. Peters, *Biol. Chem.* **2001**, *382*, 735 – 741.
[15] E. Buytaert, M. Dewaele, P. Agostinis, *Biochim. Biophys. Acta* **2007**, *1776*, 86 – 107.

